International Journal of Non-Linear Mechanics 118 (2020) 103253

Contents lists available at ScienceDirect

International Journal of Non-Linear Mechanics

journal homepage: www.elsevier.com/locate/nlm

Compact and unified elasto-plastic formulation to study isotropic plates

J.L. Mantari [a,c,*], F.G. Canales [a,b]

[a] Faculty of Mechanical Engineering, Universidad Nacional de Ingeniería (UNI), Avenida Tupac Amaru 210, Rimac, Lima, Peru
[b] D+Imac Lab, Desarrollo e investigación en mecánica aplicada y computacional, Peru
[c] Instituto de desarrollo e investigación en ingeniería naval (IDIIN), Peru

ARTICLE INFO

Keywords:
Elasto-plastic
Plasticity
Higher-order plate theories
Finite element method

ABSTRACT

We introduce a compact and unified shear deformation theory for plates with elasto-plastic behavior. We formulate the kinematics of the two-dimensional structure in a compact and unified manner using the Carrera Unified Formulation. This formulation allows for generalized expansions of the primary variables and through-the-thickness functions. We obtain the governing equations using the principle of virtual work and a finite element discretization. We solve the nonlinear equations using a Newton–Raphson linearization scheme, and linearize the constitutive equations using the algorithmic tangent moduli. We consider the J2 flow theory of plasticity, and use a backwards Euler scheme to update the stresses. We analyze the convergence, and compare the effectiveness of the Mixed Interpolation of Tensorial Components technique in contrasting the shear locking phenomenon in the nonlinear regime to the use of full and uniform reduced integration. We also conduct numerical assessments for plates under uniform and line loads. We compare the present results to those obtained by finite element commercial software, and demonstrate the computational efficiency of the present method.

1. Introduction

The elasto-plastic analysis of plates and shells is important for the design of structures subjected to extreme loads. Analytical methods are possible only for simplified geometries [1], limiting their applicability. Due to the success of the finite element method in linear analysis of plates and shells, many extensions to non-linear analyses were proposed. Then, incremental and/or iterative algorithms are used, which can be computationally expensive. In this regard, a current direction in the field is to develop formulations that are computationally efficient.

The two main approaches used for elasto-plastic analysis are lumped plasticity models and distributed plasticity models. In the lumped plasticity model, inelastic deformations are assumed to be concentrated at plastic hinge locations [2]. This method originates from limit analysis of structures [1] and is computationally efficient. However, the plastic hinge locations are assigned empirically and the results are often unreliable. On the other hand, the distributed plasticity model is known to be accurate. In that approach, the spread of plasticity is analyzed by using control points in the structure. While accurate, this approach requires discretization of the structure, making it computationally expensive. Due to this limitation, the development of efficient formulations is imperative for use in conjunction with distributed plasticity models.

Many finite element formulations have been proposed for elasto-plastic analysis of plates and shells [3–10]. These formulations often and arbitrarily assume a given displacement field. Some models are based on the Kirchhoff plate theory or the Kirchhoff–Love shell theory, which neglect transverse shear deformations. These theories are accurate for thin isotropic plates/shells, but fail as the plate/shell becomes thicker or when composite materials are considered. First-order and higher-order plate/shell theories were developed to overcome such problems. These theories are more accurate, but at the expense of computational cost. Since many different types of nonlinear variations of the displacement field along the element thickness can be considered, it is beneficial to use or develop a compact formulation that can consider any plate/shell theory in a compact and unified manner.

The Carrera Unified Formulation (CUF) allows for the development of refined plate theories in a systematic manner, as presented in Ref. [11]. Using index notation, the kinematic displacement field is assumed as a generalized expansion of element thickness displacement variables. Classical and first-order plate theories can be obtained as a special case of this unified formulation. An in-depth explanation of this formulation was provided in Refs. [12–14]. The CUF was successfully applied for structural analysis of plates with thermoelastic coupling [15,16], piezoelectric materials [17,18], functionally graded materials [19], and general multifield problems [20,21].

As is well known, the finite element method suffers from a phenomenon known as shear locking, where the analysis of thin plates requires a large amount of elements. Many different approaches were

* Correspondence to: Universidad Nacional de Ingeniería (UNI), Avenida Túpac Amaru 210, Rímac, Lima, Peru.
E-mail address: jmantaril@uni.edu.pe (J.L. Mantari).

https://doi.org/10.1016/j.ijnonlinmec.2019.103253
Received 20 September 2017; Received in revised form 12 August 2019; Accepted 12 August 2019
Available online 22 August 2019
0020-7462/

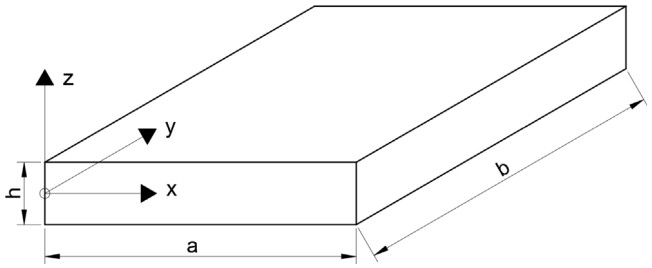

Fig. 1. Plate coordinate frame.

used to alleviate this phenomenon. Reduced and selective-reduced integration procedures were successfully applied in linear and nonlinear problems [22–24], with the added advantage of reduced computational cost. However, these techniques also produce spurious energy modes. A remedy to shear locking that does not introduce spurious modes involves introducing an assumed shear strain field, also known as the Mixed Interpolation Tensorial Components (MITC) technique. This was first proposed for the linear four nodes' plate element [25], but subsequent research works extended it to plate and shell elements with higher interpolation orders [26–30]. More recently, the MITC technique was applied in conjunction with the Carrera Unified Formulation to develop accurate analysis of plates [31,32] and shells [33–37] in the linear elastic regime. The extension of CUF to consider material and geometry nonlinearities was recently developed in Refs. [38,39].

In this paper, we develop an elasto-plastic bending analysis of plates using a compact and robust formulation in the framework of CUF. We consider plate theories of arbitrary expansion orders. We use the finite element method to discretize the structure. We obtain the nonlinear governing equations via the principle of virtual work, and they are solved by a Newton–Raphson procedure. We use a consistent tangent stiffness matrix in order to improve convergence characteristics [40]. We consider a J2 flow theory of plasticity along with the Von Mises yield criterion and a radial return algorithm for stresses update for simplicity. First, we perform a convergence analyzed, where we compare results using MITC4 and MITC9 plate elements to those obtained using full and reduced integration. Finally, the numerical results demonstrate that the present formulation is capable of accurately estimate thick plate results in a computationally efficient manner compared to commercial finite element software.

2. Finite element formulation

2.1. Preliminaries

The present mathematical formulation follows a referential coordinate system with the z-axis passing through the plate thickness. The plate length and width are denoted by a and b, respectively, as shown in Fig. 1. Then, a general displacement vector is introduced:

$$\mathbf{u}(x,y,z) = \begin{Bmatrix} u_x & u_y & u_z \end{Bmatrix}^T. \tag{1}$$

The stress and strain components are expressed in vector form as

$$\begin{aligned} \boldsymbol{\sigma} &= \begin{Bmatrix} \sigma_{xx} & \sigma_{yy} & \sigma_{zz} & \sigma_{xy} & \sigma_{xz} & \sigma_{yz} \end{Bmatrix}^T, \\ \mathbf{e} &= \begin{Bmatrix} \varepsilon_{xx} & \varepsilon_{yy} & \varepsilon_{zz} & \gamma_{xy} & \gamma_{xz} & \gamma_{yz} \end{Bmatrix}^T, \\ \boldsymbol{\varepsilon} &= \begin{Bmatrix} \varepsilon_{xx} & \varepsilon_{yy} & \varepsilon_{zz} & \varepsilon_{xy} & \varepsilon_{xz} & \varepsilon_{yz} \end{Bmatrix}^T, \end{aligned} \tag{2}$$

where $\mathbf{e}$ is the vector of engineering strains and $\boldsymbol{\varepsilon}$ is the vector of mathematical strains, i.e. $\gamma_{xy} = 2\varepsilon_{xy}$. The constitutive equation in the linear regime can be written as follows:

$$\boldsymbol{\sigma} = \mathbf{C}\boldsymbol{\varepsilon}, \tag{3}$$

where $\mathbf{C}$ is a matrix of stiffness coefficients. For an isotropic material, it is given by:

$$\mathbf{C} = \begin{bmatrix} C_{11} & C_{12} & C_{13} & 0 & 0 & 0 \\ C_{12} & C_{22} & C_{23} & 0 & 0 & 0 \\ C_{13} & C_{23} & C_{33} & 0 & 0 & 0 \\ 0 & 0 & 0 & C_{44} & 0 & 0 \\ 0 & 0 & 0 & 0 & C_{55} & 0 \\ 0 & 0 & 0 & 0 & 0 & C_{66} \end{bmatrix}, \tag{4}$$

where the stiffness coefficients depend on the Young modulus E and the Poisson ratio ν as follows:

$$\begin{aligned} C_{11} = C_{22} = C_{33} &= \frac{E(1-\nu)}{(1+\nu)(1-2\nu)}, \\ C_{12} = C_{13} = C_{23} &= \frac{E\nu}{(1+\nu)(1-2\nu)}, \\ C_{44} = C_{55} = C_{66} &= \frac{E}{(1+\nu)}. \end{aligned} \tag{5}$$

Small amplitude displacements are assumed in this paper, i.e. nonlinear geometric effects are neglected. The displacement–strain relation for mathematical strains is expressed as follows:

$$\boldsymbol{\varepsilon} = \mathbf{b}_M \mathbf{u}, \tag{6}$$

where $\mathbf{b}_M$ is a linear differential operator given by:

$$\mathbf{b}_M = \begin{bmatrix} \partial_x 0 & 0 & \\ 0 & \partial_y & 0 \\ 0 & 0 & \partial_z \\ \partial_z/2 & 0 & \partial_x/2 \\ 0 & \partial_z/2 & \partial_y/2 \\ \partial_y/2 & \partial_x/2 & 0 \end{bmatrix}, \tag{7}$$

and ∂ denotes differentiation, i.e. $\partial_x = \frac{\partial(\bullet)}{\partial x}$, $\partial_y = \frac{\partial(\bullet)}{\partial y}$ and $\partial_z = \frac{\partial(\bullet)}{\partial z}$. A similar relation is obtained if engineering strains are considered:

$$\mathbf{e} = \mathbf{b}_E \mathbf{u}, \tag{8}$$

$$\mathbf{b}_E = \begin{bmatrix} \partial_x & 0 & 0 \\ 0 & \partial_y & 0 \\ 0 & 0 & \partial_z \\ \partial_z & 0 & \partial_x \\ 0 & \partial_z & \partial_y \\ \partial_y & \partial_x & 0 \end{bmatrix}. \tag{9}$$

2.2. Plate unified finite element

The displacement field is expressed within the framework of CUF as follows:

$$\mathbf{u}(x,y,z) = F_s(z)\,\mathbf{u}_s(x,y), \qquad s = 0,1,\ldots,N, \tag{10}$$

where F_s are functions of the coordinate z, N is the number of terms used in the expansion, $\mathbf{u}_s$ is the vector of the generalized displacements, and the repeated subscript "s" indicates summation. A simple polynomial expansion is used to determine the functions F_s. For example, the displacement field of the second-order ($N = 2$) expansion model is expressed as:

$$\begin{aligned} u &= u_0 + zu_1 + z^2 u_2, \\ v &= v_0 + zv_1 + z^2 v_2, \\ w &= w_0 + zw_1 + z^2 w_2. \end{aligned} \tag{11}$$

Reduced plate order theories can be obtained by using a suitable expansion order and eliminating certain displacement variables. For example, the Mindlin plate theory is obtained by imposing kinematic constraints in a first-order expansion ($N = 1$), resulting in the following displacement field:

$$\begin{aligned} u &= u_0 + zu_1, \\ v &= v_0 + zv_1, \\ w &= w_0, \end{aligned} \tag{12}$$

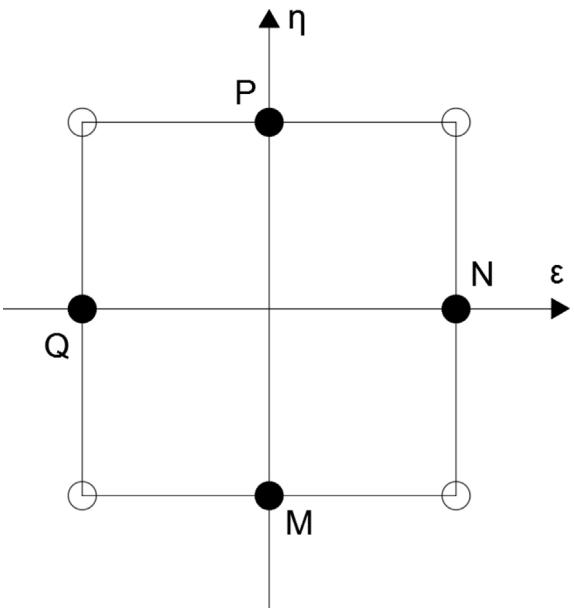

Fig. 2. Tying points for the MITC4 plate finite element.

where the displacement variables u_1 and v_1 represent rotations in the y- and x-axis respectively.

In this paper, the unified plate finite element method is used to discretize the structure along the x- and y-axis. The generalized displacements are approximated as follows:

$$\mathbf{u}_s(x,y) = N_j(x,y)\,\mathbf{q}_{sj}, \qquad j = 1,2,\ldots,p, \tag{13}$$

where p is the number of nodes of the finite element and the repeated index "j" indicates summation. $\mathbf{q}_{sj}$ is a vector of nodal parameters given by:

$$\mathbf{q}_{sj} = \left\{ q_{xsj} \quad q_{ysj} \quad q_{zsj} \right\}^T. \tag{14}$$

The shape functions N_j can be found in any standard text of finite element method, e.g. in Bathe [41].

2.3. The MITC technique

The Mixed Interpolation Tensorial Component (MITC) method calculates certain strains in a different manner from other tensorial components. For a four-noded plate finite element, the application of the MITC technique is denoted as MITC4. Following Ref. [25], the transverse shear strains are calculated as follows:

$$\begin{Bmatrix} \varepsilon_{xz} \\ \varepsilon_{yz} \end{Bmatrix} = \begin{Bmatrix} \frac{1}{2}(1+\eta)\,\varepsilon_{xz}^{P} + \frac{1}{2}(1-\eta)\,\varepsilon_{xz}^{M} \\ \frac{1}{2}(1+\xi)\,\varepsilon_{xz}^{N} + \frac{1}{2}(1-\xi)\,\varepsilon_{xz}^{Q} \end{Bmatrix}, \tag{15}$$

where (ξ,η) are the isoparametric coordinates associated with the global coordinates (x,y) and P, M, N, Q are tying points (see Fig. 2). These tying points are used as superscripts on the strains $(\varepsilon_{xz}, \varepsilon_{yz})$; they indicate an evaluation of the physical strains obtained by Eq. (6) on the corresponding sampling point.

When a nine-noded finite element is used, a new interpolation scheme is required, denoted as MITC9. Following Ref. [41], we use three different sets of tying points to interpolate the strains, as shown in Fig. 3. The interpolation functions are Lagrange polynomials, arranged as follows:

$$\begin{aligned} N_{m1}(\xi,\eta) &= \begin{bmatrix} N_{A1} & N_{B1} & N_{C1} & N_{D1} & N_{E1} & N_{F1} \end{bmatrix}, \\ N_{m2}(\xi,\eta) &= \begin{bmatrix} N_{A2} & N_{B2} & N_{C2} & N_{D2} & N_{E2} & N_{F2} \end{bmatrix}, \\ N_{m3}(\xi,\eta) &= \begin{bmatrix} N_P & N_Q & N_R & N_S \end{bmatrix}. \end{aligned} \tag{16}$$

Each Lagrange polynomial is obtained according to the location of the tying point, see Fig. 3. For example, the interpolation function N_{A1} is given by:

$$N_{A1}(\xi,\eta) = \frac{5\sqrt{3}}{12}\eta\left(\eta - \sqrt{\frac{3}{5}}\right)\left(\frac{1}{\sqrt{3}} - \xi\right). \tag{17}$$

Using these interpolation functions, the strain components are interpolated as follows:

$$\begin{bmatrix} \varepsilon_{xx} \\ \varepsilon_{yy} \\ \varepsilon_{zz} \end{bmatrix} = \begin{bmatrix} N_{m1} & 0 & 0 \\ 0 & N_{m2} & 0 \\ 0 & 0 & 1 \end{bmatrix} \begin{bmatrix} \varepsilon_{xx}^{m1} \\ \varepsilon_{yy}^{m2} \\ \varepsilon_{zz} \end{bmatrix},$$

$$\begin{bmatrix} \varepsilon_{xy} \\ \varepsilon_{xz} \\ \varepsilon_{yz} \end{bmatrix} = \begin{bmatrix} N_{m3} & 0 & 0 \\ 0 & N_{m1} & 0 \\ 0 & 0 & N_{m2} \end{bmatrix} \begin{bmatrix} \varepsilon_{xy}^{m3} \\ \varepsilon_{xz}^{m1} \\ \varepsilon_{yz}^{m2} \end{bmatrix}, \tag{18}$$

where the superscripts $(m1, m2, m3)$ on the strains indicates an evaluation of the physical strains, obtained via Eq. (6), on each of the tying points of the given set. The grouping of tying points given in Eq. (16) follows.

2.4. Governing equations

We use the principle of virtual work to obtain the governing equations:

$$\delta W_{\text{int}} - \delta W_{ext} = 0, \tag{19}$$

where δW_{int} and δW_{ext} are the virtual variations of the internal and external virtual work respectively. The variation of the internal virtual work is given by:

$$\delta W_{\text{int}} = \int_V \delta\boldsymbol{\varepsilon}^T \boldsymbol{\sigma}\, dV, \tag{20}$$

where V is the volume of the plate element. Substituting Eqs. (8), (10) and (13) into Eq. (20), we express the internal virtual work within the framework of CUF as follows:

$$\delta W_{\text{int}} = \left(\delta \mathbf{q}_{\tau i}\right)^{\text{T}} \int_V \left(\mathbf{b}_E{}^T F_\tau N_i\right) \boldsymbol{\sigma}\, dV. \tag{21}$$

The nodal internal forces are now recognized, given as follows:

$$\mathbf{f}_{\text{int}}^{\tau i} = \int_V \left(\mathbf{b}_E{}^T F_\tau N_i\right) \boldsymbol{\sigma}\, dV. \tag{22}$$

The repeated superscript "τ" and "i" are related to the variation terms, complementary to "s" and "j" used for the displacement field formulation, Eq. (10). A global internal force vector $\mathbf{f}_{\text{int}}$ can be assembled from $\mathbf{f}_{\text{int}}^{\tau i}$ by expanding the indexes $\tau = 0,1,2,\ldots,N$ and $i = 1,2,\ldots,p$ according to Eqs. (10) and (13):

$$\left(\mathbf{f}_{\text{int}}\right)^{\text{T}} = \left\{ \mathbf{f}_{\text{int}}^{11} \quad \ldots \quad \mathbf{f}_{\text{int}}^{1p} \quad \mathbf{f}_{\text{int}}^{21} \quad \ldots \quad \mathbf{f}_{\text{int}}^{2p} \quad \ldots \quad \mathbf{f}_{\text{int}}^{Mp} \right\}^{\text{T}}. \tag{23}$$

The external virtual work accounts for surface, line and point loads. Expressions for the external virtual work within the framework of CUF can be found in Ref. [11]. For example, for a vertical surface load applied on the top surface ($z = h/2$), the variation of the external virtual work is given by:

$$\delta W_{\text{ext}} = \int_{A_P} P\,\left(\delta u_z\right)\Big|_{z=h/2} dA_P, \tag{24}$$

where P is the magnitude of the surface load per unit of area and A_P is the area where the load is applied. By substituting Eqs. (10) and (13) into Eq. (24), the following expression is found:

$$\delta W_{ext} = \left(\delta q_{z_{\tau i}}\right) \int_{A_P} P\,\left(F_\tau N_i\right)\Big|_{z=h/2} dA_P, \tag{25}$$

where the nodal external forces is obtained:

$$\mathbf{f}_{\text{ext}}^{\tau i} = \int_{A_P} P\,\left(F_\tau N_i\right)\Big|_{z=h/2} dA_P. \tag{26}$$

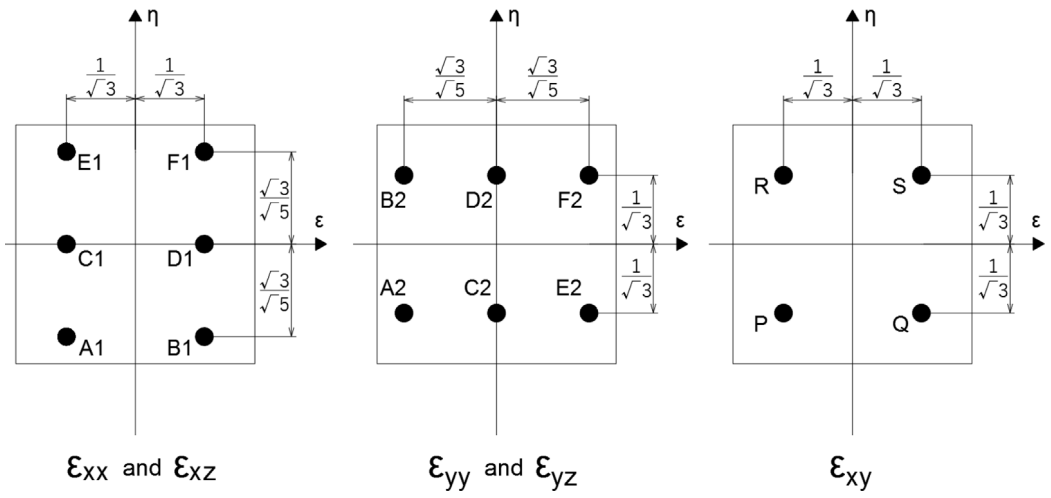

Fig. 3. Tying points for the MITC9 plate finite element.

A global external force vector $\mathbf{f}_{\text{ext}}$ can be obtained in a similar manner as the global internal force vector by using Eq. (23). Since the virtual displacements are arbitrary, Eq. (19) is equivalent to a balance of internal and external forces. By using the global force vectors, the equilibrium is expressed in the following form:

$$\mathbf{f}_{\text{int}} - \mathbf{f}_{\text{ext}} = \mathbf{0}. \tag{27}$$

2.5. Linearization

We obtain a linear system with the displacements as variables by substituting Eqs. (22) and (26) into Eq. (27) and expressing the stress vector $\boldsymbol{\sigma}$ as a function of the displacements. However, if elasto-plastic behavior is considered, the stresses are not linear with the strains and the resulting equations are nonlinear in nature. The Newton–Raphson procedure is then used to solve the equations, incrementally. In this procedure, an initial approximation is assumed and its estimated value is refined using the residual of the governing equations, i.e. the error in the governing equations obtained when the approximate solution is substituted. The residual of Eq. (27) is defined by:

$$\mathbf{r} = \mathbf{f}_{\text{int}} - \mathbf{f}_{\text{ext}}. \tag{28}$$

Using a Taylor expansion of the residual about an initial displacement approximation $\mathbf{q}_0$ and by setting the resulting expression equal to zero, we find an important relation:

$$\mathbf{r}_0 + \frac{\partial \mathbf{r}}{\partial \mathbf{q}} \Delta\mathbf{q} = 0, \tag{29}$$

where $\mathbf{r}_0 = \mathbf{r}\left(\mathbf{q}_0\right)$. The matrix $\partial\mathbf{r}/\partial\mathbf{q}$ is the effective tangent stiffness matrix of the system. Considering small amplitude displacements, the nodal external forces do not contribute to the effective tangent stiffness matrix since changes in surface area or orientation are neglected. Thus, only the internal forces contribute to the effective tangent stiffness matrix. The resulting matrix is the tangent stiffness matrix $\mathbf{K}_{\text{T}}$, which is deeply discussed in Section 2.6. Using this matrix, we express Eq. (29) as follows:

$$\mathbf{r}_0 + \mathbf{K}_{\text{T}} \Delta\mathbf{q} = 0, \tag{30}$$

where

$$\mathbf{K}_{\text{T}} = \frac{\partial \mathbf{f}_{\text{int}}}{\partial \mathbf{q}}. \tag{31}$$

Eq. (30) is the linearized model of the governing nonlinear equations. In order to obtain the complete nonlinear response, we divide the load into load steps, and solve the nonlinear system for each load step. The converged displacements from the previous load step are used as the starting value of the displacements $\mathbf{q}_0$, from which the residual $\mathbf{r}_0$ and the tangent stiffness matrix $\mathbf{K}_{\text{T}}$ are calculated. The vector $\Delta\mathbf{q}$ is obtained from the linear system in Eq. (30), and it is used to update the displacements, i.e. $\mathbf{q} = \mathbf{q}_0 + \Delta\mathbf{q}$. Afterwards, $\mathbf{r}_0$ and $\mathbf{K}_{\text{T}}$ are recalculated, and the procedure is repeated. This iterative procedure is continued until the convergence criterion is met. In this paper, the residual error is used as a criterion of convergence, where the L^2 norm of the vectors is used:

$$\frac{\|\mathbf{r}\|_{L^2}}{\max\left(\|\mathbf{f}_{\text{int}}\|_{L^2}, \|\mathbf{f}_{\text{ext}}\|_{L^2}\right)} \leq \text{TOL}, \tag{32}$$

where TOL is the error tolerance.

2.6. Tangent stiffness matrix

An expression for $\mathbf{K}_{\text{T}}$ is required in order to apply the iterative procedure mentioned above. According to Eq. (22), an increment of the internal forces is given by:

$$\text{d}\left(\mathbf{f}_{\text{int}}^{\tau i}\right) = \int_{\text{V}} \left(\mathbf{b}_E{}^T F_\tau N_i\right) \text{d}\boldsymbol{\sigma}\, \text{d}V. \tag{33}$$

Since the stress and strain are not linearly related, a linearization of the constitutive equation is required. An increment of the stress vector is related to an increment of the mathematical strain vector via the elasto-plastic modulus C^{ep}:

$$\text{d}\boldsymbol{\sigma} = \mathbf{C}^{\text{ep}} \text{d}\boldsymbol{\varepsilon}. \tag{34}$$

The procedure to obtain the elasto-plastic modulus is discussed in Section 2.7. Substituting Eqs. (34), (6), (10) and (13) into Eq. (33), we obtain the following expression:

$$\text{d}\left(\mathbf{f}_{\text{int}}^{\tau i}\right) = \text{d}\left(\mathbf{q}_{sj}\right) \int_V \left(\mathbf{b}_E{}^T F_\tau N_i\right) \mathbf{C}^{\text{ep}} \left(\mathbf{b}_M{}^T F_s N_j\right) \text{d}V, \tag{35}$$

where the repeated indices "s" and "j" indicate summation. Using Eq. (35) with Eq. (21), the tangent stiffness matrix is obtained as follows:

$$\mathbf{K}_{\text{T}}^{\tau s ij} = \int_V \left(\mathbf{b}_E{}^T F_\tau N_i\right) \mathbf{C}^{\text{ep}} \left(\mathbf{b}_M{}^T F_s N_j\right) \text{d}V, \tag{36}$$

where $\mathbf{K}_{\text{T}}^{\tau s ij}$ is the fundamental nucleus of the tangent stiffness matrix. By varying the indices "τ" and "s" of the nucleus over the range $\tau, s = 0, 1, 2, \ldots, N$, we arrive at the following matrix:

$$\mathbf{K}_{\text{T}}^{ij} = \begin{bmatrix} \mathbf{K}_{00ij} & \cdots & \mathbf{K}_{0Nij} \\ \cdots & \mathbf{K}_{\tau sij} & \cdots \\ \mathbf{K}_{N0ij} & \cdots & \mathbf{K}_{NNij} \end{bmatrix}. \tag{37}$$

Then the global tangent stiffness matrix is obtained by varying the indices "i" and "j" over the range $i, j = 1, 2, \ldots, p$:

$$\mathbf{K}_{\mathrm{T}} = \begin{bmatrix} \mathbf{K}_{11} & \cdots & \mathbf{K}_{1p} \\ \cdots & \mathbf{K}_{ij} & \cdots \\ \mathbf{K}_{p1} & \cdots & \mathbf{K}_{pp} \end{bmatrix}. \tag{38}$$

For more details about the matrix assembly using fundamental nuclei within CUF framework, the reader may consult the work by Carrera et al. [14]. According to CUF, explicit expressions of the stiffness matrix are given by decoupling integrations in the plate thickness direction and the plate longitudinal axes. However, in the present work it is not possible to decouple the integrals in the stiffness matrix because the matrix $\mathbf{C}^{\mathrm{ep}}$ varies spatially along all three axes.

2.7. Elasto-plastic modulus

In this section, we present the procedure to obtain $\mathbf{C}^{\mathrm{ep}}$. It is required when yielding occurs, according to a certain yield criterion. Note that in the elastic regime, $\mathbf{C}^{\mathrm{ep}} = \mathbf{C}$. Either the continuum or the algorithmic tangent modulus can be used in Eq. (34) to linearize the constitutive equation. Then we use the algorithmic modulus for its improved convergence characteristics. Assuming J2 flow theory of plasticity, the algorithmic tangent modulus is derived as in Ref. [40]:

$$\mathbf{C}^{\mathrm{ep}} = \mathbf{C} - 2Gb\boldsymbol{I}^{\mathrm{DEV}} - 2G(\gamma - c)\,\mathbf{S}, \tag{39}$$

where $G = E/2(1+\nu)$ is the shear modulus, $\boldsymbol{I}^{\mathrm{DEV}}$ is the deviatoric matrix and $\mathbf{S}$ is a matrix constructed using the unit deviatoric stress tensor. Expressions for $\boldsymbol{I}^{\mathrm{DEV}}$ and $\mathbf{S}$ are given in Appendix. The parameters c and γ are:

$$c = 1 - \frac{\overline{\sigma}}{\overline{\sigma} + 3G\Delta\lambda}, \quad \gamma = \frac{1}{1 + (H/3G)}, \tag{40}$$

where $\overline{\sigma}$ is the Von Mises equivalent stress, $\Delta\lambda$ is the accumulated equivalent plastic strain and H is the plastic modulus. In order to evaluate H, the instantaneous slope of the stress–strain curve E_T (evaluated at the current equivalent stress) is required. The plastic modulus is given by:

$$H = \frac{E_T E}{E - E_T}. \tag{41}$$

2.8. Stress update algorithm

Explicit schemes can be used to update the stress and plastic strain variables. However, it is often the case that the updated values do not satisfy the yield condition at the next step. This causes the solution to drift from the yield surface, resulting in inaccurate solutions. In order to avoid drifting from the yield surface, the implicit backward Euler scheme is used to obtain the plastic strains and stresses. This is an iterative procedure that enforces the yield criterion $f\left(\overline{\sigma}, \Delta\lambda\right) = 0$, at the end of the step. For the J2 flow theory of plasticity considered here, this general algorithm reduces to the well-known radial return algorithm. For more details, see Refs. [40] and [42].

Note that the stress update procedure is an inner loop of the Newton–Raphson iteration. If a bilinear stress–strain relation is assumed, then the method converges with a single iteration. Since the stress update algorithm is used on discrete points, a question arises as to where to define the monitoring points. The integral in Eq. (36) involves the elasto-plastic modulus $\mathbf{C}^{\mathrm{ep}}$, which depends on the plastic strains. For this reason, the plastic strains are evaluated at the plate element Gauss points. In this manner, $\mathbf{C}^{\mathrm{ep}}$ can be computed at these monitoring points and the integral in Eq. (36) is evaluated using Gaussian integration. We discuss the number of Gauss points used in the plate element in the next section. The complete solution algorithm is shown in Fig. 4.

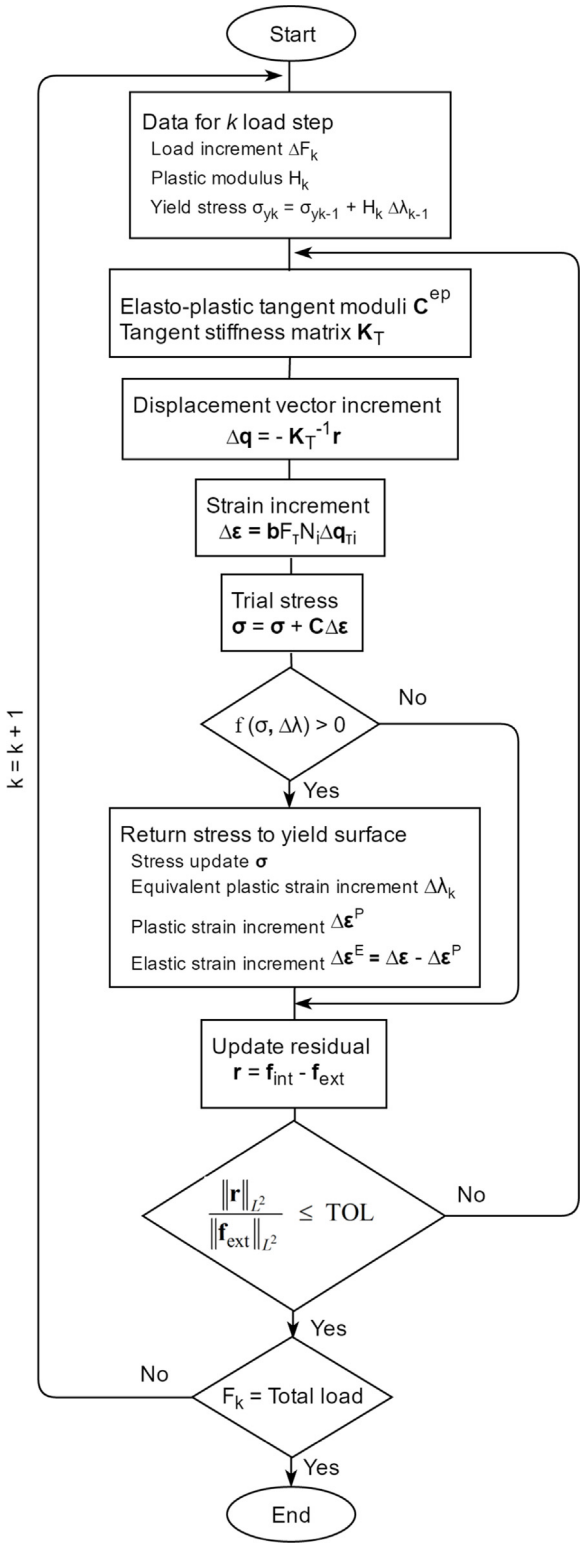

Fig. 4. Flow chart for the solution algorithm.

3. Results and discussion

3.1. Preliminaries

Here we study the accuracy of the present formulation, coded in MATLAB for all the numerical results presented in this paper. In all the numerical examples, the elastic material properties are $E = 210$ GPa

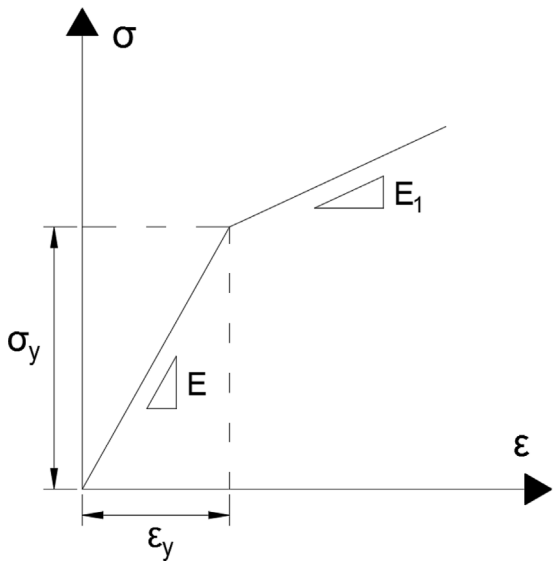

Fig. 5. Bilinear strain hardening elasto-plastic behavior.

and $\nu = 0.3$. A bilinear isotropic hardening model is assumed with $E_1 = 70$ GPa and $\sigma_Y = 350$ MPa, as shown in Fig. 5. The error tolerance used in Eq. (32) as a convergence criterion for the Newton–Raphson procedure is TOL $= 2.5 \times 10^{-3}$. The loads used are divided into 20 load steps in order to evaluate the full nonlinear response.

The number of Gauss points in the thickness of the plate is defined so that the integration of terms $F_\tau F_s$ can be performed exactly. In this manner, the stiffness matrix in the elastic regime is correctly evaluated. For example, for a model or theory with expansion order $N = 4$, the term z^8 must be integrated. Then, 5 Gauss points are used along the plate thickness. Along the plate longitudinal axes, the number of Gauss points is defined according to the interpolation order of the element, which depends on the number of nodes. If full integration is performed for a plate element with 9 nodes (quadratic interpolation), then 3 Gauss points are used along each of the plate longitudinal axes. In the case of reduced integration, only 2 Gauss points per plate longitudinal axis are used.

3.2. Measure of computational cost

For the numerical results presented in this paper, we ascertain the accuracy and computational efficiency of the present formulation by using the ANSYS commercial finite element software as a basis of comparison. The degrees of freedoms (DOFs) are used as a measure for the evaluation of the computational cost. The present formulation for a model with an expansion order N (composed of $n \times n$ plate finite element with $p \times p$ nodes each) has the following number of DOFs:

$$\text{DOF}_{\text{PRESENT}} = 3\,(N+1)\,[n\,(p-1)+1]^2\,. \tag{42}$$

In a model constructed in ANSYS using the 3D element SOLID186, each node has three translational degrees of freedom. So, the total number of DOFs is given by the number of nodes of the model multiplied by 3. Denoting the number of nodes of the ANSYS model by $\text{nodes}_{\text{ANS3D}}$, we obtain the number of DOFs as:

$$\text{DOF}_{\text{ANS3D}} = 3 \times \text{nodes}_{\text{ANS3D}}. \tag{43}$$

On the other hand, for a model built in ANSYS using the 2D element SHELL281, each node has six degrees of freedom: three translations and three rotations [43]. Then, the total number of DOFs is given by the number of nodes of the model multiplied by 6.

Table 1
Convergence of transverse displacement $\bar{u}_z$ at (x = 0.5, y = 0.5, z = 0) for a square plate with $a = b = 1$ m and $a/h = 5$ subjected to a surface load $P = 200$ MPa using full integration.

No. of plate elements	Plate theory order		
	N = 2	N = 3	N = 4
2 × 2	3.316	3.342	3.330
3 × 3	3.435	3.496	3.526
4 × 4	3.574	3.677	3.695
5 × 5	3.647	3.741	3.774
6 × 6	3.719	3.787	3.831
7 × 7	3.757	3.828	3.872
8 × 8	3.791	3.860	3.909
9 × 9	3.815	3.881	3.930
10 × 10	3.836	3.898	3.952
11 × 11	3.851	3.913	3.965
12 × 12	3.865	3.925	3.980

Table 2
Convergence of transverse displacement $\bar{u}_z$ at (x = 0.5, y = 0.5, z = 0) for a square plate with $a = b = 1$ m and $a/h = 5$ subjected to a surface load $P = 200$ MPa using nine-noded finite elements and various integration methods.

No. of plate elements	Integration method		
	Reduced	Full	MITC9
3 × 3	4.173	3.526	3.700
4 × 4	4.174	3.695	3.765
6 × 6	4.079	3.831	3.855
8 × 8	4.083	3.909	3.916
10 × 10	4.084	3.952	3.955

Table 3
Convergence of transverse displacement $\bar{u}_z$ at (x = 0.5, y = 0.5, z = 0) for a square plate with $a = b = 1$ m and $a/h = 5$ subjected to a surface load $P = 200$ MPa using four-noded finite elements and various integration methods.

No. of plate elements	Integration method		
	Reduced	Full	MITC4
4 × 4	4.029	2.547	3.105
6 × 6	4.127	3.122	3.491
8 × 8	4.089	3.386	3.628
10 × 10	4.127	3.541	3.702
12 × 12	4.079	3.651	3.769
14 × 14	4.084	3.731	3.822
16 × 16	4.081	3.785	3.858

Table 4
Convergence of transverse displacement $\bar{u}_z$ at (x = 0.5, y = 0.5, z = 0) for a square plate with $a = b = 1$ m and $a/h = 100$ subjected to a surface load $P = 2$ MPa using nine-noded finite elements and various integration methods.

No. of plate elements	Integration method		
	Reduced	Full	MITC9
3 × 3	3.101	1.597	2.445
4 × 4	3.102	2.022	2.532
6 × 6	3.060	2.470	2.669
8 × 8	3.054	2.641	2.754
11 × 11	3.050	2.765	2.832

3.3. Convergence and comparison of integration methods

We consider a square plate with dimensions $a = b = 1$ m, and a side-to-thickness ratio $a/h = 5$, where all the edges are clamped. A uniform load of magnitude $P = 200$ MPa is applied at the top surface $z = h/2$. This load drives the plate into the elasto-plastic regime. Table 1 presents the convergence of the scaled transverse displacement $u_z \times 10^3$ at (x = 0.5, y = 0.5, z = 0) as the number of finite element is increased. Nine-noded plate elements are used and the full integration scheme is performed. The displacement converges monotonically, and the results are stable for all the expansion orders N considered. The expansion order $N = 4$ is considered for further numerical examples since it provides results closer to 3D (accuracy is expected to increase with

Table 5
Convergence of transverse displacement $\bar{u}_z$ at (x = 0.5, y = 0.5, z = 0) for a square plate with $a = b = 1$ m and $a/h = 100$ subjected to a surface load $P = 2$ MPa using four-noded finite elements and various integration methods.

No. of plate elements	Integration method		
	Reduced	Full	MITC4
4 × 4	3.067	0.009	1.767
6 × 6	3.065	0.019	2.235
8 × 8	3.066	0.034	2.398
10 × 10	3.056	0.059	2.511
12 × 12	3.055	0.094	2.592
14 × 14	3.055	0.139	2.648
16 × 16	3.054	0.192	2.692

higher order plate theories). Consequently, further investigation on the convergence characteristics on this expansion order is warranted.

We also assess the usefulness of other integration methods for thick plates in the elasto-plastic regime. Again, we take the same plate geometry and material properties as the previous example with 9-node finite elements. However, uniform reduced integration and the MITC9 technique are now evaluated, in addition to the full integration method. Table 2 presents the convergence (expansion order $N = 4$) of the scaled transverse displacement $u_z \times 10^3$ at (x = 0.5, y = 0.5, z = 0) as the number of 9-node finite elements is increased. It can be seen that the MITC9 technique has accelerated convergence compared to the full integration method, although the difference decreases, as the mesh is refined. On the other hand, when using uniform reduced integration, the convergence is fast, although the monotonic convergence characteristic is lost. Table 3 presents the convergence of the scaled transverse displacement $u_z \times 10^3$ for the same case study, but using 4-node finite elements. The MITC4 technique is applied according to Eq. (15). We observe similar trends with respect to 9-node finite elements. The advantage of using MITC4 over full integration is slightly better than when MITC9 is compared with full integration. However, uniform reduced integration gives superior convergence rates.

Next, we consider a thin plate in order to evaluate the capabilities of the MITC technique and the reduced integration method to deal with shear locking in the elasto-plastic regime. We take a square plate with the same dimensions but with a side-to-thickness ratio $a/h = 100$ (thin plate) and clamped all the edges. A uniform load of magnitude $P = 2$ MPa is applied at the top surface $z = h/2$. As before, the magnitude of the load is chosen so that elasto-plastic response is obtained. Table 4 presents the convergence of the scaled transverse displacement $u_z \times 10^1$ at (x = 0.5, y = 0.5, z = 0) as the number of 9-node finite elements is increased. The shear locking phenomenon increases the difference between using full integration and the MITC9 technique compared to the case with $a/h = 5$. However, the reduced integration seems to be superior, although further research activities in the topic covered by this paper need still to be performed. Table 5 presents the convergence of the scaled transverse displacement but using 4-node element. The effects of shear locking are clear in this case, where the use of full integration results in very low displacements. On the other hand, when the MITC4 element is used, the displacement converges at much faster rate, although slower than when reduced integration is used.

Previous research on the use of MITC plate elements within the framework of CUF (using higher order plate theories) has shown convergence characteristics similar to those obtained with reduced integration methods [31]. However, in this paper only the linear elastic regime is assessed. The present section pretends to illustrate the behavior of MITC4 and MITC9 elements in the elasto-plastic regime for higher order plate theories. The results indicate that MITC elements are less effective at dealing with shear locking in this case. Consequently, the uniform reduced integration method is further used.

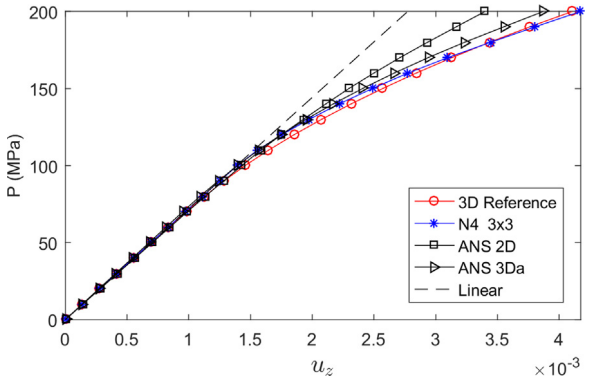

Fig. 6. Displacement–load curve for a square plate with $a = b = 1$ m and $a/h = 5$ subjected to surface loading at $z = h/2$.

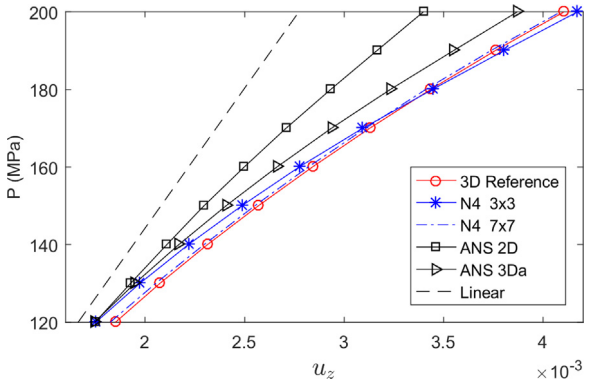

Fig. 7. Closer view of Fig. 4 in nonlinear region.

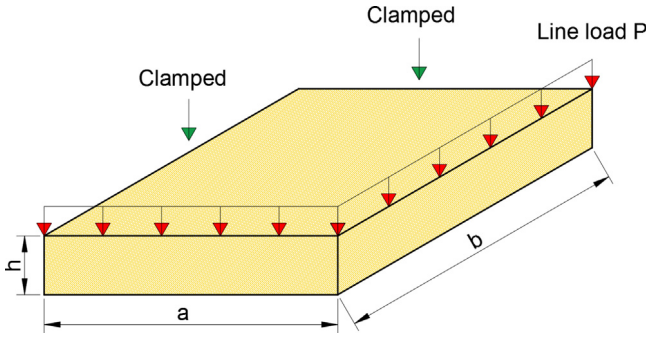

Fig. 8. Plate geometry and boundary conditions for second numerical example.

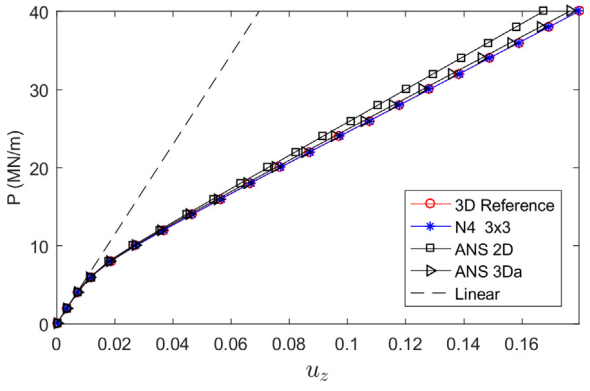

Fig. 9. Displacement–load curve for a square plate with $a = b = 1$ m and $a/h = 5$ subjected to line loads.

Table 6
Comparison of transverse displacement $\bar{u}_z$ at (x = 0, y = L, z = b/2) for a square plate with $a = b = 1$ m and $a/h = 5$ subjected to surface loading at $z = h/2$.

Model	DOFs	P (MPa)					Avg. error (%)
		120	140	160	180	200	
3D Reference	6 834 411	1.851	2.313	2.841	3.434	4.105	–
N4 3 × 3	735	1.753	2.217	2.774	3.444	4.173	2.75%
ANS 2D	798	1.740	2.096	2.490	2.929	3.400	11.93%
N4 7 × 7	3 375	1.825	2.296	2.820	3.410	4.088	0.81%
ANS 3Da	3 795	1.746	2.169	2.662	3.232	3.870	5.96%
ANS 3Db	76 539	1.833	2.290	2.810	3.397	4.058	1.06%

Table 7
Comparison of transverse displacement $\bar{u}_z$ at (x = a/2, y = L, z = b/2 − t) for a square plate with $a = b = 1$ m and $a/h = 5$ subjected to various line loads.

Model	DOFs	P (MN/m)					Avg. error (%)
		24	28	32	36	40	
3D Reference	1310 499	0.971	1.177	1.383	1.589	1.795	–
N4 3 × 3	735	0.973	1.178	1.384	1.589	1.795	0.08%
ANS 2D	798	0.914	1.103	1.293	1.483	1.672	6.43%
ANS 3Da	3 795	0.954	1.156	1.358	1.561	1.763	1.78%
ANS 3Db	45 708	0.968	1.173	1.378	1.584	1.789	0.34%

3.4. Plate subjected to uniform surface loading

In the present section, we compare results obtained by the present formulation with those of the ANSYS finite element software. We take a square plate with dimensions $a = b = 1$ m and with clamped edges. A uniform load of magnitude $P = 200$ MPa is applied at the top surface $z = h/2$. In order to demonstrate the capabilities of the present formulation to deal with thick plates, we consider a side-to-thickness ratio $a/h = 5$. We obtain results in the present formulation by using an expansion order $N = 4$ and for various mesh sizes with n finite elements along each longitudinal axis (denoted by $n \times n$). For example, a model N4 7×7 indicates a model with expansion order $N = 4$ and 7 elements along each plate longitudinal axis, resulting in 49 finite elements in total. On the other hand, results using ANSYS software with either a 2D mesh of SHELL281 elements or a 3D mesh of SOLID186 elements are obtained.

Table 6 presents values of the scaled displacement $u_Z \times 10^3$ at the geometric center of the plate as the load is increased. In order to evaluate the accuracy and computational efficiency of the present formulation, we used different finite element models:

- ANS2D is constructed using a 6 × 6 mesh with SHELL281 elements, resulting in 133 nodes and 798 DOFs.
- ANS3Da is built using a 10 × 10 × 2 mesh with SOLID186 elements, resulting in 1265 nodes and 3795 DOFs.
- ANS3Db is composed of a 30 × 30 × 6 mesh with SOLID186 elements, resulting in 25 513 nodes and 76 539 DOFs.
- The 3D reference model is constructed using a very refined mesh of 140 × 140 × 28 SOLID186 elements. This model is used as a reference to calculate the average error of the other models.

The present N4 3×3 model has similar DOFs as the ANS2D model, but much higher accuracy. This is because the 2D shell element used by ANSYS is inadequate for the elasto-plastic thick plate analyzed in this paper. Similarly, the N4 7×7 model has similar DOFs as the ANS3Da model, but much higher precision. A more refined 3D solid model with many more DOFs, ANS3Db, is required to obtain similar precision and accuracy. The computational efficiency of the present model is evident from these results.

Fig. 6 shows the load–displacement curve, as obtained by various models. The N4 3×3 model presents results closer to the 3D reference solution than others. Fig. 7 shows a closer view of the load–displacement curve in the nonlinear regime. The present N4 7×7 model is good to reproduce the nonlinear response accurately, more so than the ANS3Da model (which has a similar number of DOFs).

3.5. Plate subjected to line loading

We consider a plate with dimensions $a = b = 1$ m. The edges at $x = 0$ and $y = b$ are clamped, while the other two are free (Fig. 8). Line loads of equal magnitude $P = 40$ MN/m are applied at the edges $x = a$ and $y = 0$. Table 7 presents values of the scaled displacement $u_Z \times 10^1$ at (x = a, y = 0, z = 0) as the magnitude of the line loads is increased. The finite element models are the same as those used in Section 3.4, except for the 3D reference model, which is slightly less refined. The following remarks can be made:

- Both the present and ANSYS models have less difficulty obtaining accurate results for this case.
- The present N4 3×3 model has lower DOFs and higher accuracy than all the other models.

Fig. 9 shows the load–displacement curve for this case. The N4 3×3 model results are closer to the 3D reference solution than the other models. In addition, it can be seen that this case has a higher nonlinear response than the case analyzed previously. We observe large displacements, and the geometrical nonlinearity should be considered. This kind of nonlinearity should be further considered in future works. Remarkable works that consider nonlinearities as in Refs. [38,39,44] should be further utilized for comparison purposes.

4. Conclusions

We developed a unified formulation of plate theories with nonlinear material behavior. We compared results using different integration methods and MITC elements. In addition, we performed a comparison with commercial finite element software. The following conclusions arise from this paper:

- The present formulation is computationally efficient compared to commercial finite element software, requiring less degrees of freedom for similar accuracy.
- MITC elements can alleviate the shear locking that occurs in thin plates. However, the effectiveness of these elements for higher order plate theories is reduced in the nonlinear regime.
- Uniform reduced integration can eliminate the shear locking and provide a fast convergence rate, albeit sacrificing some numerical stability.
- While 2D plate elements based on first-order deformation theory can give acceptable results for moderately thick isotropic plates in the linear regime, they are inadequate in the elasto-plastic regime. Either higher-order plate theories or a 3D solution are required.

Acknowledgments

This paper was written in the context of the project: “Desarrollo de un software para predecir el desempeño estructural de producto terminado en el proceso de fabricación por manufactura aditiva de materiales compuestos” founded by Cienciactiva, CONCYTEC, under the contract number N° 112-2018-FONDECYT-BM-IADT-MU. The first author of this manuscript appreciate the financial support from the Peruvian Government.

Appendix. Deviatoric matrix I^{DEV} and S

The deviatoric matrix is given by [40]:

$$\boldsymbol{I}^{\mathrm{DEV}} = \begin{bmatrix} \frac{2}{3} & -\frac{1}{3} & -\frac{1}{3} & 0 & 0 & 0 \\ -\frac{1}{3} & \frac{2}{3} & -\frac{1}{3} & 0 & 0 & 0 \\ -\frac{1}{3} & -\frac{1}{3} & \frac{2}{3} & 0 & 0 & 0 \\ 0 & 0 & 0 & 1 & 0 & 0 \\ 0 & 0 & 0 & 0 & 1 & 0 \\ 0 & 0 & 0 & 0 & 0 & 1 \end{bmatrix}.$$

In order to construct the matrix **S**, the deviatoric stress tensor $\mathbf{s}_{\mathrm{T}}$ must first be obtained by subtracting the hydrostatic part:

$$\mathbf{s}_{\mathrm{T}} = \begin{bmatrix} s_{xx} & s_{xy} & s_{xz} \\ s_{xy} & s_{yy} & s_{yz} \\ s_{xz} & s_{yz} & s_{zz} \end{bmatrix}.$$

The unit deviatoric stress tensor is obtained as:

$$\boldsymbol{\eta}_{\mathrm{T}} = \frac{\mathbf{s}_{\mathrm{T}}}{\|\mathbf{s}_{\mathrm{T}}\|} = \begin{bmatrix} \eta_{xx} & \eta_{xy} & \eta_{xz} \\ \eta_{xy} & \eta_{yy} & \eta_{yz} \\ \eta_{xz} & \eta_{yz} & \eta_{zz} \end{bmatrix},$$

where $\|\ \|$ denotes the tensor norm. For programming purposes, the second-order symmetric tensor $\boldsymbol{\eta}_{\mathrm{T}}$ is converted to an equivalent vector $\boldsymbol{\eta}$:

$$\boldsymbol{\eta} = \begin{Bmatrix} \eta_{xx} & \eta_{yy} & \eta_{zz} & \eta_{xy} & \eta_{xz} & \eta_{yz} \end{Bmatrix}^{T}.$$

The matrix **S** is defined as follows:

$$\mathbf{S} = \boldsymbol{\eta}\boldsymbol{\eta}^{\mathrm{T}}.$$

References

[1] P.G. Hodge, Plastic Analysis of Structures, McGraw-Hill, New York, 1959.
[2] Y. Ueda, T. Yao, The plastic node method: A new method of plastic analysis, Comput. Methods Appl. Mech. Engrg. 34 (1982) 1089–1104.
[3] H. Parisch, A continuum-based shell theory for non-linear applications, Internat. J. Numer. Methods Engrg. 38 (1995) 1855–1883.
[4] F.G. Flores, E. Oñate, A basic thin shell triangle with only translational DOFs for large strain plasticity, Internat. J. Numer. Methods Engrg. 51 (2001) 57–83.
[5] G. Shi, G.Z. Voyiadjis, A simple non-layered finite element for the elasto-plastic analysis of shear flexible plates, Internat. J. Numer. Methods Engrg. 33 (1992) 85–99.
[6] H. Kebari, A.C. Casell, A stabilized 9-node non-linear shell element, Internat. J. Numer. Methods Engrg. 35 (1992) 37–61.
[7] R. Hauptmann, K. Schweizerhof, A systematic development of 'solid-shell' element formulations for linear and non-linear analysis employing only displacement degrees of freedom, Internat. J. Numer. Methods Engrg. 42 (1998) 49–69.
[8] E. Turco, Elasto-plastic analysis of Kirchhoff plates by high simplicity finite elements, Comput. Methods Appl. Mech. Engrg. 190 (2000) 691–706.
[9] G. Shi, G.Z. Voyiadjis, Geometrically nonlinear analysis of plates by assumed strain element with explicit tangent stiffness matrix, Comput. Struct. 41 (1991) 757–763.
[10] H. Parisch, Large displacements of shells including material nonlinearities, Comput. Methods Appl. Mech. Engrg. 27 (1981) 183–214.
[11] E. Carrera, Theories and finite elements for multilayered plates and shells. A unified compact formulation with numerical assessment and benchmarking, Arch. Comput. Methods Eng. 10 (2003) 215–296.
[12] E. Carrera, G. Giunta, M. Petrolo, Beam Structures: Classical and Advanced Theories, Wiley, Chichester, United Kingdom, 2011.
[13] E. Carrera, S. Brischetto, P. Nali, Plates and Shells for Smart Structures: Classical and Advanced Theories for Modeling and Analysis, Wiley, Chichester, United Kingdom, 2011.
[14] E. Carrera, M. Cinefra, M. Petrolo, E. Zappino, Finite Element Analysis of Structures Through Unified Formulation, Wiley, Chichester, United Kingdom, 2014.
[15] E. Carrera, Transverse normal strain effects on thermal stress analysis of homogeneous and layered plates, AIAA J. 43 (2005).
[16] A. Robaldo, E. Carrera, A. Benjeddou, Unified formulation for finite element thermoelastic analysis of multilayered anisotropic composite plates, J. Therm. Stresses 28 (2005) 1031–1065.
[17] A. Robaldo, E. Carrera, A. Benjeddou, A unified formulation for finite element analysis of piezoelectric adaptative plates, Comput. Struct. 84 (2006) 1494–1505.
[18] E. Carrera, M. Boscolo, A. Robaldo, Hierarchic multilayered plate elements for coupled multifield problems of piezoelectric adaptative structures: Formulation and Numerical Assessment, Arch. Comput. Methods Eng. 14 (2007) 383–430.
[19] E. Carrera, S. Brischetto, A. Robaldo, Variable kinematic model for the analysis of functionally graded material plates, AIAA J. 46 (2008).
[20] E. Carrera, S. Brischetto, P. Nali, Variational statements and computational models for multifield problems and multilayered structures, Mech. Adv. Mater. Struct. 15 (2008) 182–198.
[21] E. Carrera, S. Brischetto, C. Fagiano, P. Nali, Mixed multilayered plate elements for coupled magneto-electro-elastic analysis, Multidiscip. Model. Mater. Struct. 5 (2009) 251–256.
[22] O.C. Zienkiewicz, R.L. Taylor, J.M. Too, Reduced integration technique in general analysis of plates and shells, Int. J. Numer. Methods Eng. 3 (1971) 275–290.
[23] J.R. Hughes, M. Cohen, M. Haroun, Reduced and selective integration techniques in the finite element analysis of plates, Nucl. Eng. Des. 46 (1978) 203–222.
[24] J.R. Hughes, Generalization of selective integration procedures to anisotropic and nonlinear media, Internat. J. Numer. Methods Engrg. 15 (1980) 1413–1418.
[25] K.J. Bathe, E.N. Dvorkin, A four-node plate bending element based on Mindlin/Reissner plate theory and a mixed interpolation, Internat. J. Numer. Methods Engrg. 21 (1985) 367–383.
[26] H.C. Huang, E. Hinton, A new nine node degenerated shell element with enhanced membrane and shear interpolation, Internat. J. Numer. Methods Engrg. 22 (1986) 73–92.
[27] H.C. Huang, Membrane locking and assumed strain shell elements, Comput. Struct. 27 (1987) 671–677.
[28] J. Jang, P.M. Pinsky, An assumed covariant strain based 9-node shell element, Internat. J. Numer. Methods Engrg. 24 (1987) 2389–2411.
[29] C. Chinosi, L.D. Croce, Mixed-interpolation elements for thin shells, Int. J. Numer. Methods Biomed. Eng. 14 (1998) 1155–1170.
[30] K.J. Bathe, P.S. Lee, J.F. Hiller, Towards improving the MITC9 shell element, Comput. Struct. 81 (2003) 477–489.
[31] E. Carrera, M. Cinefra, P. Nali, MITC technique extended to variable kinematic multilayered plate elements, Compos. Struct. 92 (2010) 1888–1895.
[32] C. Chinosi, M. Cinefra, L.D. Croce, E. Carrera, Reissner's mixed variational theorem toward MITC finite elements for multilayered plates, Compos. Struct. 99 (2013) 443–452.
[33] M. Cinefra, C. Chinosi, L.D. Croce, MITC9 shell elements based on refined theories for the analysis of isotropic cylindrical structures, Mech. Adv. Mater. Struct. 20 (2013) 91–100.
[34] M. Cinefra, C. Chinosi, L.D. Croce, E. Carrera, Refined shell elements based on RMVT and MITC for the analysis of laminated structures, Compos. Struct. 113 (2014) 492–497.
[35] M. Cinefra, S. Valvano, E. Carrera, A layer-wise MITC9 finite element for the free vibration analysis of plates with piezo-patches, Int. J. Smart Nano Mater. 6 (2015) 85–104.
[36] M. Cinefra, S. Valvano, E. Carrera, Thermal stress analysis of laminated structures by a variable kinematic MITC9 shell element, J. Therm. Stresses 39 (2016) 121–141.
[37] M. Filippi, M. Petrolo, S. Valvano, E. Carrera, Analysis of laminated composites and sandwich structures by trigonometric, exponential and miscellaneous polynomials and a MITC9 plate element, Compos. Struct. 150 (2016) 103–114.
[38] E. Carrera, I. Kaleel, M. Petrolo, Elastoplastic analysis of compact and thin-walled structures using classical and refined beam finite element models, Mech. Adv. Mater. Struct. (2017) http://dx.doi.org/10.1080/15376494.2017.1378780.
[39] A. Pagani, E. Carrera, Unified formulation of geometrically nonlinear refined beam theories, Mech. Adv. Mater. Struct. 25 (1) (2018) 15–31.
[40] T. Belytschko, W.K. Liu, B. Moran, K.I. Elkhodary, Nonlinear Finite Elements for Continua and Structures, Wiley, Chichester, United Kingdom, 2014.
[41] Klaus-Jürgen Bathe, Finite Element Procedures, Prentice Hall, New Jersey, US, 1996.
[42] J.C. Simo, R.L. Taylor, Consistent tangent operators for rate-independent elastoplasticity, Comput. Methods Appl. Mech. Engrg. 48 (1985) 101–118.
[43] ANSYS Inc. ANSYS Mechanical APDL Theory Reference, SAS IP, Canonsburg, US, 2013.
[44] M. Abambres, D. Camotim, N. Silvestre, GBT-based first-order analysis of elastic–plastic thin-walled steel members exhibiting strain-hardening, IES J. A: Civ. Struct. Eng. 6 (2) (2013) 119–134.